TEMPERATURE DEPENDENT DIELECTRIC AND ELECTRICAL CHARACTERISTICS OF RARE EARTH SUBSTITUTED SBT CERAMIC

S. Devi [1], G. K. Sahu[2], S. Behera[2]* , S. R. Mishra[3].

[1] *Department of Physics, Gandhi Engineering College, Bhubaneswar, Odisha, India*
[2]*Department of Physics, Centurion University of Technology and Management, Bhubaneswar, India.*
[3]*Department of Chemistry, Gandhi Institute for Education and Technology, Baniatangi, Bhubaneswar, Odisha.*

Abstract

The $Sr(Bi_{0.9}Y_{0.1})_2Ta_2O_9$ ceramic was prepared by standard SSR method at an optimized calcination temperature (1000^0C). Formation of single-phase compound with orthorhombic crystal structure is confirmed from XRD pattern. The temperature variation of dielectric constant exhibits improved thermal stability (TCC) behaviors useful for MLCC applications. The room temperature hysteresis loop confirms the ferroelectric property of the material with good remnant polarization applicable for memory device. Complex impedance spectroscopy is used to determine the distinct components in the corresponding electrical circuit. The fact that ac conductivity changes with temperature indicates that the conduction mechanism is a thermally triggered process. Conduction occurs in the ceramics due to the long-range mobility of single -ionized oxygen vacancies. The thermistor parameters are calculated at higher temperature for NTC thermistor applications.

Keywords: **Dielectric; X-ray diffraction; TCC, Complex Impedance; Ferroelectricity; Thermistor.**

1. INTRODUCTION

Ferroelectrics with Bismuth layered structure like $SrBi_2Ta_2O_9$ (SBT), $SrBi_2Nb_2O_9$ (SBN) are important materials for temperature stable memory devices (FRAMs) [1-6]. In particular, SBT is widely explored due to its excellent properties like extended cycling with polarization fatigue reduced or alleviated polarization fatigue up to 10^{12} cycles, low switching voltage, good ferroelectric properties (large P_r values) and low leakage current [2]. It is known that by suitable stoichiometric change in both bulk and thin film of SBT ceramics, the dielectric and ferroelectric properties can be modified [7,8]. Some groups have attempted to improve the remnant polarization of SBT ceramic by modifying the composition[9,10]. Senthil et al. reported the effect of rare earth Y^{3+} substitutions in Sr^{2+} site on the ferroelectric, electrical and photocatalytic behavior of SBT ceramics[11]. The improvement of ferroelectric behavior of SBT ceramics by rare-earth doping in Sr^{2+} and Bi^{3+} is also reported by others [12,13]. In literature it is known that the ferroelectric and electrical behaviors of BLSF structures are strongly determined by Bi_2O_2 layers. The modifications in dielectric and ferroelectric properties of SBT ceramic by appropriate replacement of Bi^{3+} ions by lanthanide cations are explored earlier [14]. Some efforts are also reported on the rare earth doping on Bi sites for LED applications [15,16]. So, it is concluded that rare-earth doping in the Bi sites is effective for improvement of useful properties. This paper discusses the characteristics behaviour of Yttrium (Y) substituted SBT ceramic. We have adopted a trial method by slowly increasing the calcination temperature followed by phase conformation after each interval to optimize the minimum formation temperature.

2. Experimental methods

The high purity oxides (>99.9%): $SrCO_3$, Bi_2O_3, Y_2O_3 and Ta_2O_5 are used as starting raw materials which are weighed according to the stoichiometric ratio with the $Sr(Bi_{0.9}Y_{0.1})_2Ta_2O_9$ abbreviated as SBYT and ground in an agate mortar for 2 h. The mixed powder is ball milled in a laboratory ball milling machine using Zr ball in acetone medium. 3 wt% of excess Bi_2O_3 is added with calculated precursors to compensate the loss during sintering. The mixed precursors are calcined at 1273K for 4 h after drying acetone. Then the calcined powder is ground in agate mortar and mixed with polyvinyl alcohol (PVA) (Merck KGaA, 64271 Darmstadt.) which act as a binder for preparation of the disk. The powder is uniaxially pressed into circular disks of 10-12 mm in diameter and 1-1.5 mm in thickness and sintered at 1473K for 1 h with a heating rate of 5K/min. The end faces of the sintered pellets are made parallel and flat using fine emery paper. The phase formation of the sintered pellets is structurally characterized using X-ray diffraction (XRD) (PANalytical, Japan) and surface morphology of the sintered pellet is studied using Scanning electron microscope, (JEOL, USA). In order to measure the electrical properties, disk surfaces are polished uniformly and coated with silver paste (Coatex Industries) for electroding purpose. After electroding the pellet was dried for 1 h at 473K to remove the moisture if present and was cooled to room temperature before taking any electrical measurement. Temperature dependence dielectric data are measured from 300K to 673K with the rising temperature of 1K/min using Salatron 1260 gain/phase analyzer, Germany. The hysteresis is studied using P–E loop tracer (Radient Technology, USA).

3. Result and Discussion

3.1. Structural and morphological analysis

The XRD pattern of the sintered pellet of SBYT ceramic is presented in Figure 1. The observed peaks and lattice parameter were redefined using X'Pert high score computer Software program. The XRD analysis reveal the grown materials have single-phase Bi-layered ($m = 2$) Aurivillius compounds with $A2_1am$ orthorhombic symmetry, which is consistent with standard XRD database (JCPDS: 49-0609). The sharp and distinguished peaks confirm the formation of new single-phase material. The derived lattice parameters are $a = 5.6208$Å, $b = 5.5263$Å and $c = 25.0232$Å. In the XRD patterns, a strong (115) diffraction line at about $2\theta \approx 28.39°$ is detected, which indicates polarization along the a-axis direction [11].

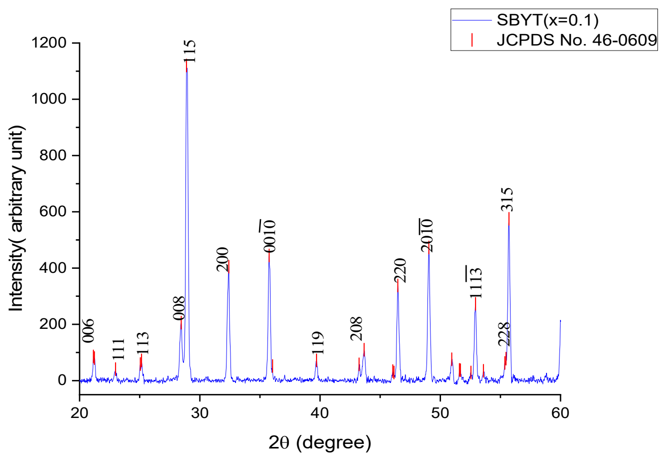

***Figure 4.1**: XRD patterns of the SBYT ceramic (x=0.1)*

3.2 Microstructural Analysis

Figure 2 gives the surface morphology of the sintered pellet of Y substituted SBT ceramic. The distinctive features of bismuth layer compounds are clearly observed from the grain morphologies of the ceramic. The sample exhibits anisotropy, and the grains have a rod-like shape with minimal porosity. The bulk density of sintered pellets is found to be 95-97% of the theoretical density. The SEM micrographs manifest the polycrystalline nature of the SBYT ceramics.

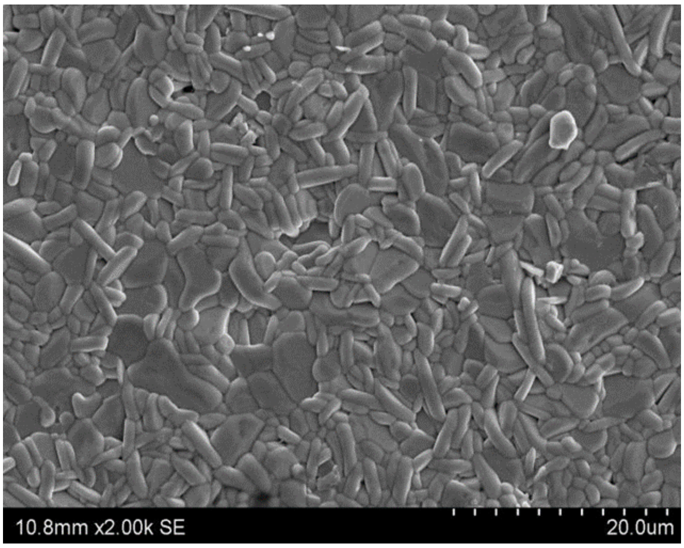

***Figure 2**: Surface morphology of the SBYT ceramic*

3.3. Dielectric properties

The dielectric permittivity (ε_r) of SBYT ceramic varies with temperature (Figure 3) at selected frequencies in a similar behaviour of other Bismuth layered structure ferroelectrics [17-20]. The reduction in both dielectric constant and ferroelectric phase transition with the substitution excess amount of Yttrium is an indication of the development of ionic bond (Y–O) from covalent bond (Bi–O) in the Bi_2O_2 layer [21] . Additionally, the lowering of both the dielectric parameters (ε_r and T_C) is explained in terms of reduction of TaO_6 octahedron distortion of SBT ceramics. The unit cell dimension and lattice deviation of the parent SBT ceramic increases because of incorporation of the cation Y^{3+} having a larger covalent radius as compared to Bi^{3+}. The lone pair of $6s^2$ electrons present in Bi^{3+} ion actively participate in induction of dipole moment (polarization) in the perovskite layers of SBT structure as compared to bonded electron pairs. Consequently, the absenteeism of lone pair of electrons in the lanthanide cation (Y^{3+}) reduces the net induced polarization and B site octahedral distortion. Again, according to Shannon (1993) the room temperature polarizability for Bi^{3+} is more than Y^{3+}. From Clausius- Mossotti relation the lower polarizability will shift the T_m and T_C lower temperature site. Again, it is also stated that doping with small cationic radius in A site of SBT ceramics creates more rattling space resulting more dielectric constant with high transition temperature although amalgamation of large ionic radius fallouts a converse effect [22,23]. So, both the maximum dielectric constant (ε_m) and transition temperatures (T_C) fall down with substitution of Y. Lowering of maximum dielectric constant values with doping has a noteworthy effect on improvement of remnant polarization in SBT based ceramics useful for memory applications. The frequency dependent T_C or strict relaxor behaviour is not observed in the composition because of absence of nano sized polar regions (PNR) in them resulting from their large grain size. As it is known that this PNR are responsible for relaxor behavior in Bi based perovskites [24]

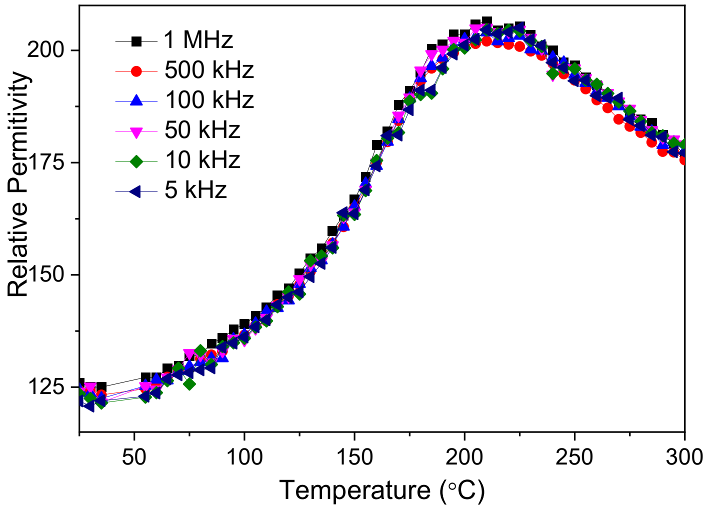

***Figure 3**: Temperature variation of dielectric constant at various frequency*

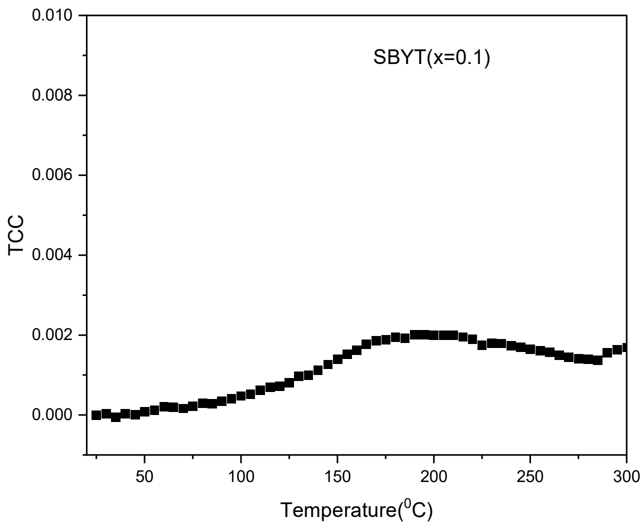

***Figure 4**: Variation of TCC of SBYT ceramic with temperature at 50 KHz*

The dielectric constant of the Y modified ceramic shows negligible variation with temperature up to 300^0C indicating excellent thermal stability. The thermal stability of the materials is related to the capacitance (C) and is expressed by the temperature coefficient of capacitance (TCC). The temperature coefficient of dielectric constant TCC (τ_ε) is calculated using the formula

$$\tau_\varepsilon = (\varepsilon_T - \varepsilon_{RT})/\varepsilon_{RT}\Delta T$$

where ΔT =measuring temperature (T)-room temperature (RT) and ε_{RT} is the room temperature dielectric constant. The units of TCC is parts per million (ppm)^{o}C^{-1} and TCC ≈ 0 indicates high thermal stability of the materials as capacitors. The TCC was calculated for the sample within temperature range (25-300)^{0}C and presented in Fig. 4. In the above temperature range the values of τ_ε are close to zero which reflects the suitability of the materials for microwave resonators and MLCC application.

The broad dielectric peaks specify the presence of second order phase transitions in these materials with broadening confirmed by conniving the degree of diffuseness (γ) from the temperature variation of dielectric constant using the modified Curie–Weiss law [25]:

$$\frac{1}{\varepsilon} - \frac{1}{\varepsilon_m} = \frac{(T - T_m)^\gamma}{C'} \qquad (\text{at } T > T_m) \qquad (4.1)$$

where C' is a constant, γ has values between 1 and 2. The values of γ indicate classical Curie Weiss law and an ample diffuse phase transition respectively. The corresponding γ values are calculated from the slopes of the plot between logarithm of $(1/\varepsilon - 1/\varepsilon_m)$ and logarithm of $(T - T_C)$ at 50 kHz (Figure 5).

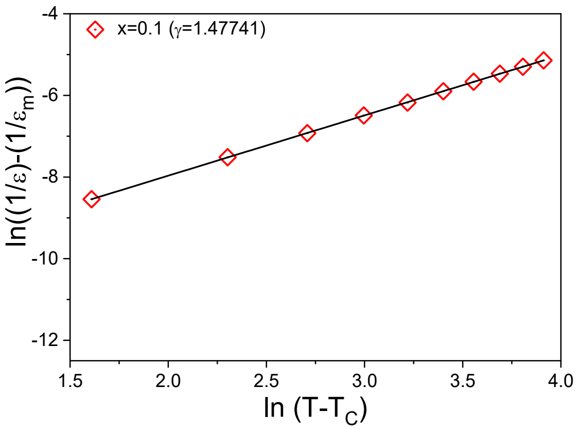

***Figure 5**: Relationship between logarithm of $(1/\varepsilon - 1/\varepsilon_m)$ and logarithm of $(T - T_C)$ at 50 kHz for SBYT ceramic.*

The presence of more than two no of cations in the A site of the perovskite layers is responsible for such type of phase transition in it. It is also reported earlier that doping of rare earths in Bi-site of BLSF structure predisposed the dielectric constant with wide peak because of the nonuniform dispersal of rare earths in layered structure [26,27]. The presence of diffuse phase transition in the material is confirmed from the values of γ (degree of diffusivity) as 1.47 (between 1 to 2).

3.4 Ferroelectric properties

The assumed ferroelectric behaviour of the Yttrium modified SBT ceramic is confirmed from the polarization reversal curves (hysteresis loop) shown in Figure 6. The closed hysteresis loop in this figure confirms the assumed ferroelectric nature in the dielectric plot. The observed good remnant polarization (P_r) in the material aligns it for memory applications. In the process of high temperature sintering stoichiometric loss occurs in the pure SBT material due to volatilization of Bi_2O_3 leaving some oxygen vacancies in terms of inherent defects [28]. Substituting an isovalent lanthanoid cation for Bi^{3+} at the A-site reduces bismuth vacancies and stabilises oxygen ions in the perovskite layers [29]. These oxygen vacancies (V_o) work as space charge resulting strong pinning of the domains causing less P_r values [30,31]. With the addition of the trivalent ion (Y^{3+}), to maintain the structure's overall charge neutrality, cation vacancies are produced in the A-site. Hence the dopant ion behaves as a donor reducing the oxygen vacancies and the pinning effect on the domain walls with a larger contribution of P_r to the parent materials [32]. It is also anticipated that the polarization increases due to Y^{3+} doping as a result of increase of no of switchable domain in the presence of electric field [6].

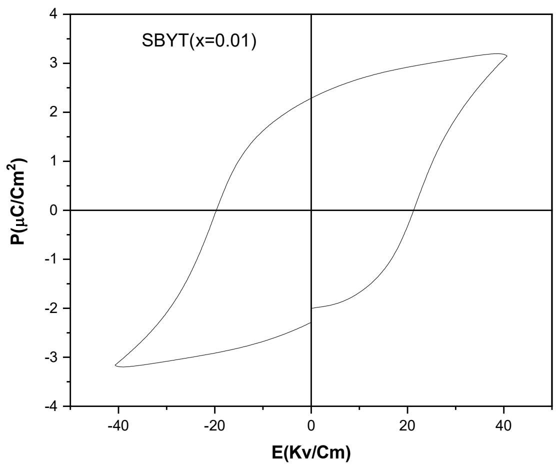

***Figure 6**: The P–E hysteresis loops of SBYT ceramic.*

3.5 AC conductivity

The AC conductivity of SBYT ceramic as function of frequency (5kHz-1MHz) at different temperatures is shown in Figure 7. The graph is divided into three sections with varying slopes: (i) low frequency dispersion, (ii) intermediate frequency (plateau) dispersion, and (iii) high frequency conductivity dispersion. In the low frequency (space-charge) region, the polarisation effect causes variations in conductivity. The long-range translational motion of ions contributing to dc conductivity (σ_{dc}) is ascribed to the frequency independent plateau at moderate frequency [33]. The charts show that the material's conductivity increases as the temperature rises. Also, the dispersion is readily evident at lower frequencies, while the curves blend at higher frequencies. In the high frequency range, however, conductivity rises at all temperatures when the slope changes. The hopping frequency is the rate at which the slope varies. With rising temperature, the hopping frequency changes to the upper side, as seen in the graph [34].As the temperature rises, a frequency independent zone (plateau region) stretches to the higher frequency and relaxes into a strong dispersive region. The plateau zone results from long-range charge carrier movement, while the dispersive region results from localised or short-range charge carrier movement, resulting in ac conduction. As a result, the relaxation frequency is determined by the point at which dc to ac conduction occurs [35]. Jonscher's power law [36] governs this kind of frequency dependent conductivity s(u) spectrum:

$$\sigma_{ac} = \sigma_{dc} + A\omega^n \qquad (4.2)$$

where σ_{dc} is the DC conductivity (corresponding to the frequency-independent plateau in the low-frequency region), A is a frequency pre-exponential factor which depends on temperature, and n is the power-law exponent ($0 \leq n \leq 1$). The preexponential factor (A) controls the intensity of the polarizability, whereas the power n denotes the degree of interaction between mobile ions and the lattice surrounding them. It is clear that σ_{ac} rises with frequency, although it is practically independent in the low-frequency area. σ_{dc} is obtained by extrapolating this component towards the lower frequency side. The rising tendency of σ_{ac} with increasing frequency (in the low frequency area) might be explained by cation disorder between surrounding sites or the existence of space charge [37]. The curves approach each other in the high-frequency area. A low-frequency dispersion phenomenon following Jonscher's power law is shown by the conductivity charts. The origin of the frequency dependence of conductivity, according to Jonscher, is related to relaxation events caused by mobile charge carriers. A mobile charge carrier stays in a condition of displacement between two potential energy minima as it hops to a new site from its initial location.

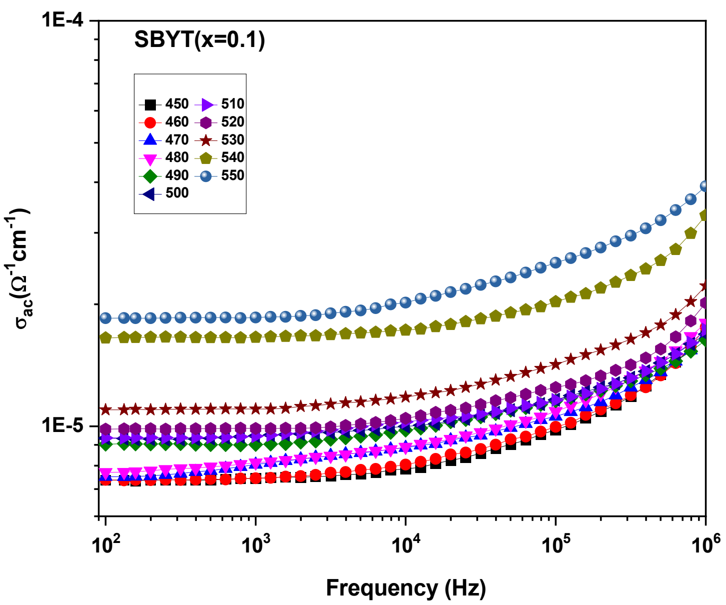

***Figure** 7: Frequency dependence AC conductivity at different temperature for SBYT ceramic.*

3.6 Complex impedance analysis

Impedance spectroscopy is a good way to link the electrical properties of heterogeneous polycrystalline materials to their microstructure. The complex impedance (Z) is generally expressed as:

$$Z = Z' + jZ'' \tag{1}$$

where Z' and Z'' are the resistive and the reactive part of the impedance. This section describes the frequency and temperature dependent components of impedance for the material. The numerous contributions made in the system can be quantified by fitting the impedance data with an analogous electrical circuit. Figures 8(a &b) demonstrate the frequency dependent real impedance (Z') and imaginary impedance (Z'') for SBYT ceramic at the temperature range of 450-550°C. Because of the release of space charge induced by a decrease in barrier characteristics as temperature rises, the Z' values for all temperatures blend at a high frequency. It could also explain why ac conductivity rises with temperature at high frequencies. When the frequency (log f) is increased, the Z' falls, suggesting an increase in AC conductivity. Furthermore, the nonlinear behaviour of Z' values as a function of temperature is evident. The asymmetric fluctuation in the broadness of the Z" peaks pointed to an electrical process with a relaxation time spread [38]. The presence of temperature dependent relaxation phenomenon is explained by the shifting of Z" max towards the high frequency side. The reduction in Z" with temperature shows increased conductivity due to the material's space charge. Because it takes less time for space charges to relax and recombine at high frequencies, space charge polarization decreases as frequency rises and seems to merge at high frequencies for all temperatures.

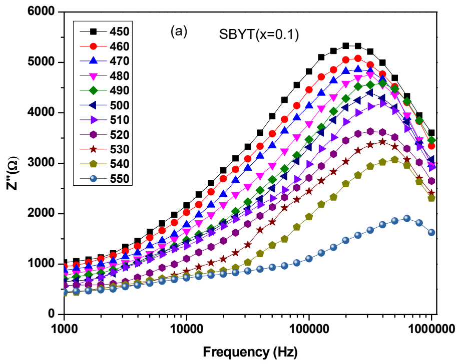

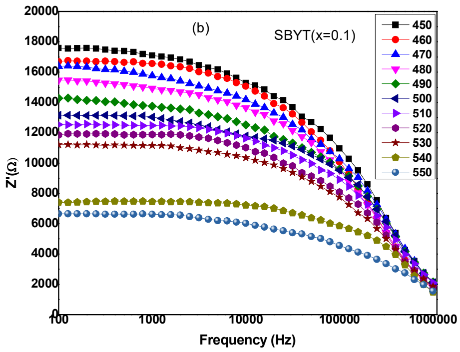

Figure 8*: Variation of impedance with frequency at different temperatures for SBYT* ***(a)*** *imaginary value of impedance (Z")* ***(b)*** *real value of impedance (Z').*

For polycrystalline materials, complex impedance spectroscopy is utilized to investigate frequency domain features (such as grain, grain boundary, and interface effects). The qualitative information regarding the contribution of grain, grain boundary, and interface effects is provided over a wide range of frequencies and temperatures. Utilizing applicable equations, one can anticipate the theoretical values of a material by using a parallel combination of resistance (R) and capacitance (C) in an equivalent electrical circuit. The fitting of impedance spectroscopy data to an equivalent electrical circuit can reveal how the system's various contributions evolved. In an analogous circuit, each parallel combination of $R - C$ must be considered for its own relaxation process.

The complex impedance spectrum (Z' vs Z") of SBYT ceramic is shown in Figure 9. The sample fits best with a series of two parallel components $RC - RQ$ or $RQ - RC$, where 'R' is resistance, 'C' is capacitance, and 'Q' is the constant phase element (CPE) indicating the electrical contributions from both grain and grain boundary[39-40] (equivalent circuit is drawn on the graph). The term CPE refers to a relaxation mechanism that is not Debye, in which the centre of a semicircle is dislocated below the axis. With increasing temperature, the radius of the semicircle shrinks, confirming the negative temperature coefficient of resistance of the material. Fig 10 shows the fitting parameters (bulk resistance) as a function of temperature for the complex impedance spectrum using SBYT ceramics equivalent circuits.

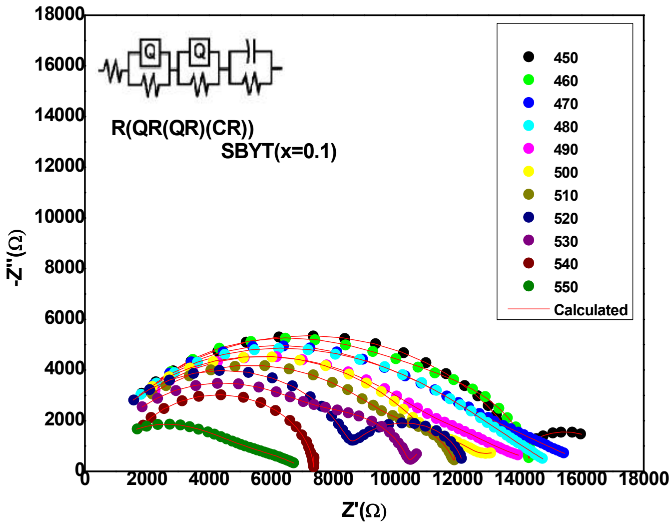

Figure 9*: Complex impedance spectrum (Z' vs Z'') of SBYT ceramic (Solid line represents respective circuit fitting).*

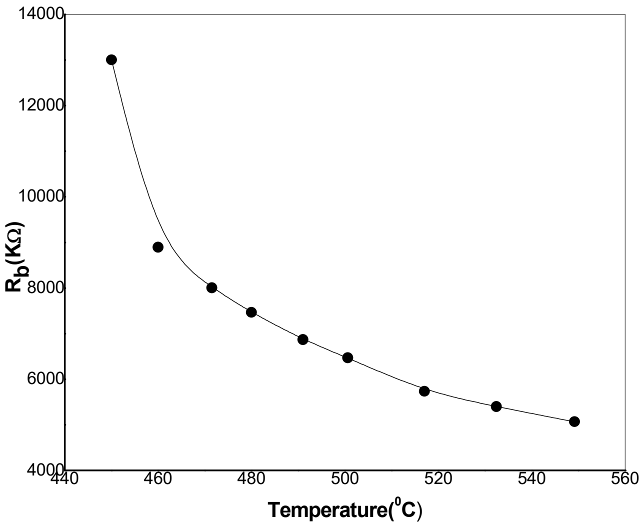

Figure 10*: Variation of bulk resistance with temperature of the ceramic.*

3.7 Thermistor Constant beta (β) or Sensitivity

It is noticed from the temperature variation of bulk resistance (Fig.10) graph that resistance follows semiconductor behavior with increasing temperature by the following exponential equation.

$$R = R_0 \exp(\frac{-E_a}{K_B T}) \quad \text{or} \quad R = R_0 \exp \beta (\frac{1}{T} - \frac{1}{T_0}) \qquad (1)$$

Where R and R_0 are the resistance of the compound at the temperature T (K) and fixed temperature T_0(K) respectively and β is material characteristic properties known as the NTC thermistor parameter.

The following equation is used to get the β value

$$\beta = \frac{ln\left(\frac{R_{T1}}{R_{T2}}\right)}{\left(\frac{1}{T_1}-\frac{1}{T_2}\right)} \quad (2)$$

Where R_{T1} and R_{T2} are the resistances at two different temperature T_1 and T_2 respectively. The thermistor specification and components are decided from the values of β [41]. The variation of β with temperature is shown in fig.11 and it directly varies with the temperature. In literature it is open that β should ranges between 4000K-15000K for use as good thermal sensor [42]. The values of β calculated for the material remain between 6000K-116000K and concludes the use of the material as high temperature NTC thermistor.

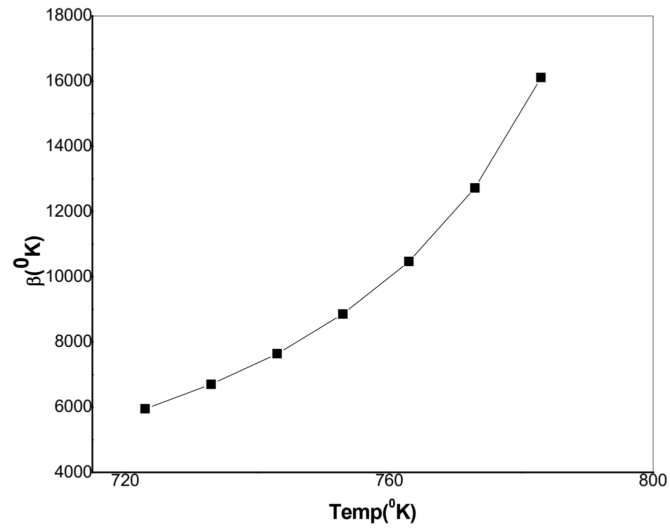

Fig.11: Variation of β with temperature.

4. Conclusion

The $Sr(Bi_{0.9}Y_{0.1})_2Ta_2O_9$ ceramic was prepared by standard SSR method. Formation of single-phase compound with orthorhombic structure is confirmed from XRD pattern. The temperature variation of dielectric constant exhibits improved dielectric behaviors with lower transition temperature values near room temperature device applications. The room temperature hysteresis loop confirms the ferroelectric property of the material with good remnant polarization applicable for memory device. Complex impedance spectroscopy is used to determine the distinct components in the corresponding electrical circuit. Conduction occurs in doped ceramics due to the long-range mobility of single -ionized oxygen vacancies. The study of temperature-dependent resistance supports SBYT as a good candidate for NTC thermistor-related device applications. The frequency variation of ac conductivity follows Josher's power law. The negligible TCC value of the material is promising for a tunable microwave device.

REFERENCES

[1] Kajewski, D. and Ujma, Z., "Electrical conductivity of $SrBi_2Ta_2O_9$ ceramics," Ceramics International **39** (7), pp. 8213-8218, 2013.

[2] Coondoo, I. and Jha, A. K., "Enhancement of ferroelectric and piezoelectric characteristics in europium substituted $SrBi_2Ta_2O_9$ ferroelectric ceramics," Materials Letters **63** (1), pp. 48-50, 2009.

[3] Kajewski, D. and Ujma, Z., "Electrical properties of $SrBi_2(Nb_{0.5}Ta_{0.5})_2O_9$ ceramics," Journal of Physics and Chemistry of Solids **71** (1), pp. 24-29, 2010.

[4] Senthil, V., Badapanda, T., Chithambararaj, A., Chandra Bose, A., and Panigrahi, S., "Impedance spectroscopy and photocatalysis water splitting for hydrogen production with cerium modified $SrBi_2Ta_2O_9$ ferroelectrics," International Journal of Hydrogen Energy **41** (48), pp. 22856-22865, 2016.

[5] Chen, Y., Du, Y., Fan, D., Niu, H., Zuo, Y., Hu, L., Liu, K., Shen, M., Shang, X., and Chen, Y., "Study on the polarization enhancement mechanism and electrical properties of high temperature bismuth layered $K_xNa_{0.5-x}Bi_{4.46}Ce_{0.04}Ti_4O_{15+y}$ ceramics," Ceramics International **47** (20), pp. 29023-29029, 2021.

[6] Chen, Y., Zhang, C.-C., Qin, L., Jiang, C.-B., Liu, K.-H., Ma, C., Wu, Z.-T., Pan, R.-K., Cao, W.-Q., Ye, C., and Li, Z., "Enhanced dielectric and piezoelectric properties in $Na_{0.5}Bi_{4.5}Ti_4O_{15}$ ceramics with Pr-doping," Ceramics International **44** (15), pp. 18264-18270, 2018.

[7] Coondoo, I., Jha, A. K., and Agarwal, S. K., "Structural, dielectric and electrical studies in tungsten doped $SrBi_2Ta_2O_9$ ferroelectric ceramics," Ceramics International **33** (1), pp. 41-47, 2007.

[8] Wang, D.-S., "Effect of annealing atmosphere on volatility of Bi in $SrBi_2Ta_2O_9$ thin films," J Ceram Process Res **15** (2), pp. 116-119, 2014.

[9] Kitamura, A., Noguchi, Y., and Miyayama, M., "Polarization properties of praseodymium-modified $SrBi_2Ta_2O_9$ ceramics and thin films prepared by sol–gel method," Materials Letters **58** (11), pp. 1815-1818, 2004.

[10] Sridarane, R., Subramanian, S., Janani, N., and Murugan, R., "Investigation on microstructure, dielectric and impedance properties of $Sr_{1-x}Bi_{2+(2/3)x}(V_xTa_{1-x})_2O_9$ [x=0, 0.1 and 0.2] ceramics," Journal of Alloys and Compounds **492** (1), pp. 642-648, 2010.

[11] Senthil, V. and Panigrahi, S., "Dielectric, ferroelectric, impedance and photocatalytic water splitting study of Y^{3+} modified $SrBi_2Ta_2O_9$ ferroelectrics," International Journal of Hydrogen Energy **44** (33), pp. 18058-18071, 2019.

[12] Wei, T., Zhao, C. Z., Zhou, Q. J., Li, Z. P., Wang, Y. Q., and Zhang, L. S., "Bright green upconversion emission and enhanced ferroelectric polarization in $Sr_{1-1.5x}Er_xBi_2Nb_2O_9$," Optical Materials **36** (7), pp. 1209-1212, 2014.

[13] Sugandha and Jha, A. K., "Effect of holmium substitution on electrical properties of strontium bismuth tantalate ferroelectric ceramics," Ceramics International **39** (8), pp. 9397-9403, 2013.

[14] Senthil, V., Badapanda, T., Chandrabose, A., and Panigrahi, S., "Dielectric and ferroelectric behavior of cerium modified $SrBi_2Ta_2O_9$ ceramic," Materials Letters **159**, pp. 138-141, 2015.

[15] Zhong, Y., Sun, P., Gao, X., Liu, Q., Huang, S., Liu, B., Deng, B., and Yu, R., "Synthesis and optical properties of new red-emitting $SrBi_2Ta_2O_9:Eu^{3+}$ phosphor application for w-LEDs commercially based on InGaN," Journal of Luminescence **212**, pp. 45-51, 2019.

[16] Zhong, Y., Deng, B., Gao, X., Sun, P., Ren, Y., Liang, T., and Yu, R., "High thermally Sm^{3+}-activated $SrBi_2Ta_2O_9$ orange-red phosphor: Preparation, characterization, and optical properties," Journal of Luminescence **215**, pp. 116648, 2019.

[17] Nayak, P., Badapanda, T., and Panigrahi, S., "Dielectric and ferroelectric properties of Lanthanum modified $SrBi_4Ti_4O_{15}$ ceramics," Materials Letters **172**, pp. 32-35, 2016.

[18] Sahu, R. and Kumar, P., "Microstructural, dielectric and ferroelectric properties of $Sr_{0.8}Bi_{2.15}Ta_2O_9$ ceramics synthesized by microwave processing technique," Phase Transitions **93** (1), pp. 91-99, 2020.

[19] Nayak, P., Badapanda, T., and Panigrahi, S., "Effect of lanthanum modification on dielectric and conduction behaviour of $SrBi_4Ti_4O_{15}$ ceramic," AIP Conference Proceedings **1832** (1), pp. 030017, 2017.

[20] Miyayama, M. and Noguchi, Y., "Polarization properties and oxygen-vacancy distribution of $SrBi_2Ta_2O_9$ ceramics modified by Ce and Pr," Journal of the European Ceramic Society **25** (12), pp. 2477-2482, 2005.

[21] Zhu, J. S., Qin, H. X., Bao, Z. H., Wang, Y. N., Cai, W. Y., Chen, P. P., Lu, W., Chan, H. L. W., and Choy, C. L., "X-ray diffraction and Raman scattering study of $SrBi_2Ta_2O_9$ ceramics and thin films with Bi_3TiNbO_9 addition," Applied Physics Letters **79** (23), pp. 3827-3829, 2001.

[22] Verma, M., Sreenivas, K., and Gupta, V., "Influence of La doping on structural and dielectric properties of $SrBi_2Nb_2O_9$ ceramics," Journal of Applied Physics **105** (2), pp. 024511, 2009.

[23] Sun, L., Feng, C., Chen, L., and Huang, S., "Dielectric and Piezoelectric Properties of $SrBi_{2-x}Sm_xNb_2O_9$ (x=0, 0.05, 0.1, 0.2, 0.3, and 0.4) Ceramics," Journal of the American Ceramic Society **90** (12), pp. 3875-3881, 2007.

[24] Praharaj, S., Rout, D., Anwar, S., and Subramanian, V., "Polar nano regions in lead free $(Na_{0.5}Bi_{0.5})TiO_3$-$SrTiO_3$-$BaTiO_3$ relaxors: An impedance spectroscopic study," Journal of Alloys and Compounds **706**, pp. 502-510, 2017.

[25] Park, B. H., Hyun, S. J., Bu, S. D., Noh, T. W., Lee, J., Kim, H.-D., Kim, T. H., and Jo, W., "Differences in nature of defects between $SrBi_2Ta_2O_9$ and $Bi_4Ti_3O_{12}$," Applied Physics Letters **74** (13), pp. 1907-1909, 1999.

[26] Afqir, M., Tachafine, A., Fasquelle, D., Elaatmani, M., Carru, J.-C., Zegzouti, A., Daoud, M., Sayouri, S., Lamcharfi, T.-D., and Zouhairi, M., "Structural, electric and dielectric properties of Eu-doped $SrBi_2Nb_2O_9$ ceramics obtained by co-precipitation route," Processing and Application of Ceramics **12** (1), pp. 72- 77, 2018.

[27] Adak, M. K., Mukherjee, A., Chowdhury, A., Khatun, J., Dhak, P., and Dhak, D., "Dielectric anomaly, diffusivity and impedance behavior of transition metal substituted $SrBi_2NbTaO_9$ ferroelectric nano-ceramics prepared by chemical route," Physica B: Condensed Matter **553**, pp. 26-35, 2019.

[28] Kannan, B. R. and Venkataraman, B. H., "Effect of rare earth ion doping on the structural, microstructural and diffused phase transition characteristics of $BaBi_2Nb_2O_9$ relaxor ferroelectrics," Ceramics International **40** (10, Part B), pp. 16365-16369, 2014.

[29] Gupta, P., Mahapatra, P. K., and Choudhary, R. N. P., "Structural and Electrical Characteristics of an Aurivillius Family Compound $Bi_2LaTiVO_9$," Crystal Research and Technology **53** (12), pp. 1800045, 2018.

[30] Noguchi, Y., Miwa, I., Goshima, Y., and Miyayama, M., "Defect Control for Large Remanent Polarization in Bismuth Titanate Ferroelectrics -- Doping Effect of Higher-Valent Cations," Japanese Journal of Applied Physics **39** (Part 2, No. 12B), pp. L1259-L1262, 2000.

[31] Friessnegg, T., Aggarwal, S., Ramesh, R., Nielsen, B., Poindexter, E. H., and Keeble, D. J., "Vacancy formation in $(Pb,La)(Zr,Ti)O_3$ capacitors with oxygen deficiency and the effect on voltage offset," Applied Physics Letters **77** (1), pp. 127-129, 2000.

[32] Coondoo, I. and Jha, A. K., "Investigations of structural, dielectric and ferroelectric behavior of europium substituted $SrBi_2Ta_2O_9$ ferroelectric ceramics," Solid State Communications **142** (10), pp. 561-565, 2007.

[33] Li, W. and Schwartz, R. W., "ac conductivity relaxation processes in $CaCu_3Ti_4O_{12}$ ceramics: Grain boundary and domain boundary effects," Applied Physics Letters **89** (24), pp. 242906, 2006.

[34] Srinivas, K., Sarah, P., and Suryanarayana, S. V., "Impedance spectroscopy study of polycrystalline $Bi_6Fe_2Ti_3O_{18}$," Bulletin of Materials Science **26** (2), pp. 247-253, 2003.

[35] Pattanayak, R., Panigrahi, S., Dash, T., Muduli, R., and Behera, D., "Electric transport properties study of bulk $BaFe_{12}O_{19}$ by complex impedance spectroscopy," Physica B: Condensed Matter **474**, pp. 57-63, 2015.

[36] Jonscher, A. K., "The 'universal' dielectric response," Nature **267** (5613), pp. 673-679, 1977.

[37] Karan, N. K., Pradhan, D. K., Thomas, R., Natesan, B., and Katiyar, R. S., "Solid polymer electrolytes based on polyethylene oxide and lithium trifluoro- methane sulfonate (PEO–$LiCF_3SO_3$): Ionic conductivity and dielectric relaxation," Solid State Ionics **179** (19), pp. 689-696, 2008.

[38] Khokhar, A., Mahesh, M. L. V., James, A. R., Goyal, P. K., and Sreenivas, K., "Sintering characteristics and electrical properties of $BaBi_4Ti_4O_{15}$ ferroelectric ceramics," Journal of Alloys and Compounds **581**, pp. 150-159, 2013.

[39] *Gupta, P., Mahapatra, P. K., and Choudhary, R. N. P., "Structural and electrical characteristics of rare-earth modified bismuth layer structured compounds," Journal of Alloys and Compounds* ***863****, pp. 158457, 2021.*

[40] *Badapanda, T., Nayak, P., Mishra, S. R., Harichandan, R., and Ray, P. K., "Investigation of temperature variant dielectric and conduction behaviour of strontium modified* $BaBi_4Ti_4O_{15}$ *ceramic," Journal of Materials Science: Materials in Electronics* ***30*** *(4), pp. 3933-3941, 2019.*

[41] *Luo W, Yao HM, Yang PH, et al. Negative temperature coefficient material with low thermal constant and high resistivity for low temperature thermistor applications. J Am Ceram Soc. 2009;92:2682–2686.*

[42]. *Mott NF. Metal insulator transitions. London: Taylor and Francis; 1990.*